Astron. Astrophys. 342, 601–609 (1999)

ASTRONOMY AND ASTROPHYSICS

Improved analysis of interplanetary HST–$H_{Ly\alpha}$ spectra using time–dependent modelings

Horst Scherer[1], **Maciej Bzowski**[2], **Hans J. Fahr**[1], **and Daniel Ruciński**[2]

[1] Institut für Astrophysik und Extraterrestrische Forschung der Universität Bonn, Auf dem Hügel 71, D-53121 Bonn, Germany
[2] Space Research Centre of the Polish Academy of Sciences, Bartycka 18 A, PL-00 716 Warsaw, Poland

Received 7 April 1998 / Accepted 25 October 1998

Abstract. During a period of 18 months 5 Hubble–Space–Telescope GHRS interplanetary $H_{Ly\alpha}$ glow spectra were obtained at different lines of sight from different positions of the earth on its orbit, but despite employment of a radiation transport model that takes into account the angle–dependent partial frequency redistribution, the self-absorption by interplanetary hydrogen, the realistic spectral profile of the solar $H_{Ly\alpha}$ emission line, and a stationary hydrogen model with a heliospheric interface, no common parameter set for density, temperature and velocity of the interstellar hydrogen could be deduced (see our earlier paper Scherer et al. 1997). One possible explanation is the uncertainty in the interstellar hydrogen inflow direction, but even this would not completely dissolve some discrepancies between the theoretical predictions of spectral Doppler shifts and those observed in the HST $H_{Ly\alpha}$ spectra. As we show here the theoretical predictions can be improved by using a time–dependent hydrogen model that also takes into account heliospheric interface effects, long–term variation of the $H_{Ly\alpha}$ irradiance, its influence on the radiation pressure and the long–term variation of the hydrogen ionisation rate. The attempt at finding a common LISM parameter set, fitting 3 HST spectra is improved, though there still remain some discrepancies between data and the theoretical description, mainly manifest over time scales of the order of a year. This residual could be explained by possible variations in the spectral shape of the solar H Ly-α line profile adopted as constant to model the radiation pressure and the resonance intensities.

Key words: inteplanetary medium – radiative transfer

1. Introduction

The solar wind consisting of electrons and protons expands from the solar corona into the heliosphere. Beyond the termination shock it interacts hydrodynamically with the local interstellar medium (LISM), a partly ionized plasma with a charged component and embedded neutrals (e.g.: H, He, O, Ne, N, C,. . .), moving towards the sun. The magnetohydrodynamical interaction of the two plasmas enforces a tangential contact discontinuity, the heliopause. Beyond the shock the solar wind approaching the heliopause is decelerated. A transition region (heliospheric interface) exists, where the solar wind plasma is subsonic. The neutral component of the LISM passes over the heliopause and the shock, influenced only indirectly by charge exchange and electron impact reactions with plasma constituents. Then it flows towards the sun with very little change of its density, bulk velocity and temperature until at some proximity to the sun the influence of solar gravity, radiation pressure and ionisation by charge exchange and electromagnetic radiation becomes significant.

In the past decades several attempts have been made to develop an appropriate stationary, kinetic description of the solar wind – LISM plasma interaction, based on different approaches like the Boltzmann integro–differential equation (e.g. Ripken & Fahr 1983, Fahr & Ripken 1984, Osterbart & Fahr 1992, Fahr 1996) or hydrodynamic approximations (Baranov & Malama 1993 Williams et al. 1996, Zank & Pauls 1996).

The hydrogen $H_{Ly\alpha}$ resonance glow acts as tracer for the LISM plasma conditions. Its integrated intensity was measured by several experiments. To interpret these $H_{Ly\alpha}$ resonance glow measurements using a radiation transport model (e.g. Keller & Thomas 1979, Keller et al. 1981, Quémerais & Bertaux 1993, Hall et al. 1993, Ajello et al. 1994, Scherer & Fahr 1996), the hydrogen density, temperature and velocity pattern in the solar vicinity, determined by appropriate models, had to be taken into account. From these interpretations the thermodynamical state of LISM hydrogen should be derivable.

Up to now, however, most of these derivations have been based on frequency–integrated glow intensity data which give added–up contributions from local radiation sources along the line of sight disregarding the spectral frequency. Because the $H_{Ly\alpha}$ resonance emission strongly varies along the line of sight, one could not reliably deduce a set of LISM parameters (see Table 1). Better information became available in the last three years from measurements of five spectrally resolved $H_{Ly\alpha}$ glow spectra with the Hubble–Space-Telescope (HST) (Clarke et al. 1995).

The data from these HST spectra show a strong variation over the time period of three years, when the spectra were observed. Therefore, the interpretation of these spectra with time–independent models (especially the hydrogen models) did not

Send offprint requests to: Horst Scherer (hscherer@astro.uni-bonn.de)

Table 1. LISM parameter, derived by several $H_{Ly\alpha}$ resonance glow measurements.

density cm^{-3}	velocity $km\,s^{-1}$	temperature K	μ	data	published
0.03–0.06	20	8000	0.75	PROGNOZ 5/6	Bertaux et al. 1985 Lallement & Bertaux 1985
0.07 ± 0.01				Mariner 10	Ajello et al. 1987
0.065 ± 0.01	19–25	7000–9000		(several instruments)	Lallement 1989
0.065–0.1	20 ± 1	8000 ± 500		Pioneer–Venus, Voyager	Lallement 1990
0.06	20 ± 1	8000 ± 1000		Voyager 1/2	Lallement et al. 1990a, 1990b
0.1–0.13				Voyager 1/2	Lallement et al. 1991
0.065	19 ± 1 (upwind) 25 ± 1 (downwind)	8000 ± 500 8000 ± 500	0.75 ± 0.1 0.75 ± 0.1	PROGNOZ 5/6	Quémerais et al. 1992
	20 ± 1	8000		HST star observation	Bertin et al. 1993
0.029–0.037	20	8000	0.75	PROGNOZ 6	Summanen et al. 1993
0.04–0.12	20	7500–12500	0.75	Voyager	Hall et al. 1993
0.17	20	8000	1.1	Galileo UV spectrometer	Ajello et al. 1994
0.135 ± 0.025	20	8000		ALAE/ATLAS 1	Quémerais et al. 1994
0.1–0.3	25	7000	1	Voyager 1/2	Quémerais et al. 1995
	20	8000		PROGNOZ 5	Bertaux et al. 1996

yet allow us to derive a common set of LISM parameters (Clarke et al. 1998, Scherer et al. 1997). Thus, only by using hydrogen models that take time–dependences due to solar cycle effects into account (e.g. Kyrölä et al. 1994, Bzowski & Ruciński 1995a, 1995b, Ruciński & Bzowski 1995, 1996, Summanen 1996, Kausch & Fahr 1997), could one hope to improve the interpretation of the HST spectra.

2. Data description

Five high resolution spectra of the interplanetary $H_{Ly\alpha}$ resonance glow from 1212.3 Å to 1218.7 Å were measured using the GHRS instrument on board the HST during a period from 1994 till 1996. Each of these spectra were taken at different lines of sight and at different times (see Table 1 in Scherer et al. 1997).

For each of the five surveys, 4–10 data sets are available (FP_SPLIT mode of the GHRS instrument), with an integration time of 544 sec each. The data sets of one survey are merged together using an IDL-language procedure, resulting in a noise-reduced spectra for every line of sight (for data handling of the GHRS instrument see Baum (1994) or Solderblom (1994)).

The strongest spectral feature in all measurements is the geocoronal $H_{Ly\alpha}$ glow (see Fig. 1). To eliminate the influence of HST's motion with respect to earth on the Doppler shift of the observed interplanetary glow line, the observed shifts of geocoronal spectra with respect to the terrestrial rest frame were used. The velocity component of the earth's ecliptic motion with respect to the instrument's line of sight was obtained by taking the derivatives of the J2000 ephemeris coordinates. The Earth–Moon motion and the sun–barycenter motion have not been taken into account, limiting the accuracy of the earth velocity component to $\pm$ 0.025 [$km\,s^{-1}$] (see Table 1 in Scherer et al. 1997 and Table 2 in this work). The residual spectral shift of the $H_{Ly\alpha}$ glow is caused by the inflow of the neutral IPM hydrogen speed and is the main object of interest in this paper.

Table 2. Results of a best fit procedure on HST data

Date	view direction	spectral maximum[1]	v_{Earth} LOS[2]	v_{IPM} LOS[2]
		[Å]	$km\,s^{-1}$	$km\,s^{-1}$
07.04.94	upwind	1215.486	−24.7	20.7
04.06.94	crosswind	1215.778	29.7	2.5
06.03.95	downwind	–[2]	29.8	–[3]
25.03.95	upwind	1215.459	−27.7	24.3
09.03.96	downwind	–[2]	29.7	–[3]

[1] Result of a best fit procedure, using a Voigt profile for fitting.
[2] velocity component along the line of sight.
[3] Bad statistics. No reliable fit possible (Fig. 1).

The spectral broadening of a point source by the instrumental environment of the GHRS, the so called point spread function (PSF), has been determined by several authors (e.g.: Clarke et al. 1995, Gilliland et al. 1992). Because the HST-GHRS $H_{Ly\alpha}$ glow data are very noisy, it is not advised to deconvolve the PSF by the data, but it is more convenient to convolve the theoretical spectra with the PSF and compare the results with the $H_{Ly\alpha}$ glow data (see Fig. 1).

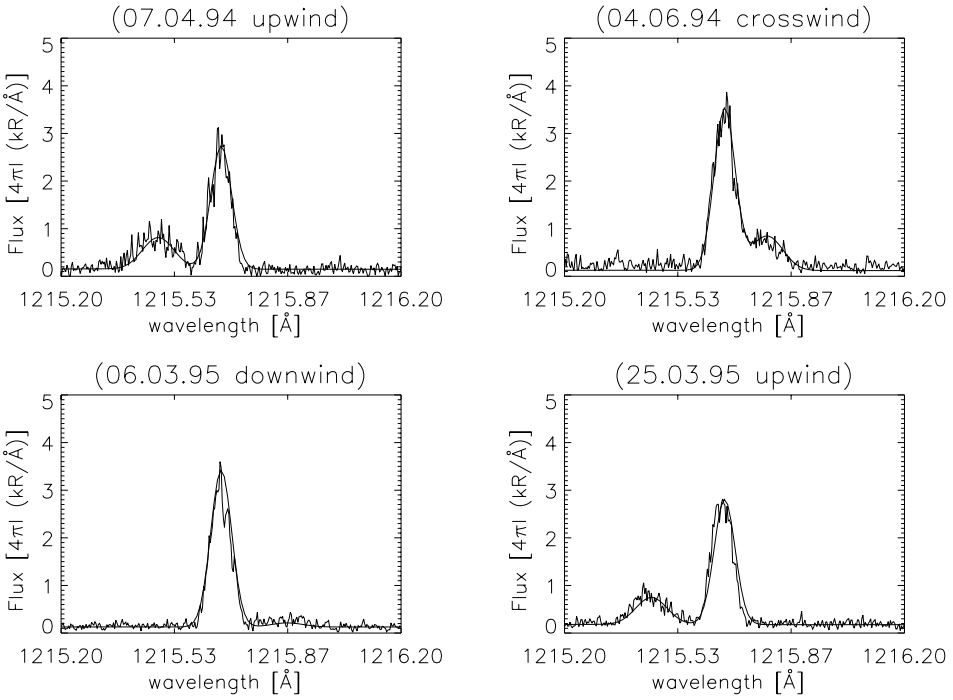

Fig. 1. HST data and result of a best fit procedure using a Voigt–profile for geocoronal and IPM $H_{Ly\alpha}$ glow. (The fifth spectrum, taken by the HST–GHRS at 09.03.96, is not shown here because it is very similar to the spectral data taken at 06.03.95. Both of the data sets have a bad statistics and no reliable data fit could be obtained.)

3. Theoretical models for the data description

3.1. Time-dependent hydrogen model

The time-dependent hydrogen model used in this study to compute the hydrogen distribution was described in Ruciński & Bzowski (1995) and Bzowski et al. (1997). The temporal courses of the ionisation rate and radiation pressure used in this modeling are presented in Fig. 3. The model radiation pressure course was developed based on full-disk, line-integrated intensity time series using AE-E, SME and UARS satellites and their cross–calibrations by Tobiska et al. (1997). In the hydrogen model calculation it was assumed that the full-disk, line-integrated solar $H_{Ly\alpha}$ flux is proportional to the flux at the line center. This assumption may not be fully valid but due to the lack of other data nothing better could be achieved. This issue will still be discussed further in the paper.

The modeled ionisation rate is a sum of the charge exchange rate computed from the IMP-8 data, available from NSSDC, and of the photoionisation rate computed from a 10.7 cm proxy discussed by Ruciński et al. (1996). From the computed charge exchange and photoionisation time series, a discrete Fourier analysis was performed (see Press and Rybicki 1989) and based on the periodicities ω_j found in the data, the following approximate formulae for both rates were fitted using a linear regression method with: $\beta = \beta_0 + \sum_{j=1}^{J} (p_j \cos\omega_j t + q_j \sin\omega_j t)$. A similar analysis was performed with the $H_{Ly\alpha}$ data.

To compute the distribution function f of hydrogen in a selected location in the inner heliosphere at a given moment of time for an arbitrary local velocity vector one needs to calculate two statistical weights attributed to a test atom: the ionisation weight $w_{\rm ion}$ and the kinematic weight $w_{\rm kin}$: $f = w_{\rm kin} \times w_{\rm ion}$. $w_{\rm kin}$ is the value of hydrogen distribution function in the so called "reference region", i.e. in a location in space where it is assumed that the physical state of the gas is known, and $w_{\rm ion}$ is the probability of survival of the test atom during its travel from the reference region to the local point. The reference region adopted in this study was a Sun-centered sphere with a diameter of ~ 200 AU (close to the distance to the nose of the solar wind termination shock).

In order to compute the statistical weights, one tracks the test atom backwards in time using the Recurrent Power Series method discussed by Ruciński & Bzowski (1995). As initial values the selected time, the position and the velocity vectors are taken. The tracking is done by solving the equation of motion in the presence of solar gravitation (constant in time) and the variable solar radiation pressure shown in Fig. 3. Along with the actual position and velocity of the atom its survival probability against ionisation is computed: $w_{\rm ion}(t) = \exp\left[-\int_{t_0}^{t} \beta\,(r(t'),t')\ {\rm d}t'\right]$. The atom is tracked back until it is within the reference region. Then the actual velocity vector is saved and the offset angle ϕ from the inflow direction is computed from the calculated position. Based on this angle, the local thermodynamic parameters of the gas are computed from precalculated approximation formulae. These formulae were derived from a twin-shock, self-consistent, static, Monte Carlo model of interaction of the LISM with the solar wind (Baranov & Malama 1993) with input parameters consistent with the mean values of μ– and β–courses adopted in the modeling. Since in this model two distinct populations of hydrogen atoms flow into the heliosphere (the so-called 'direct' and 'indirect' populations), the kinematic weight of the atom is calculated from the assumed formula

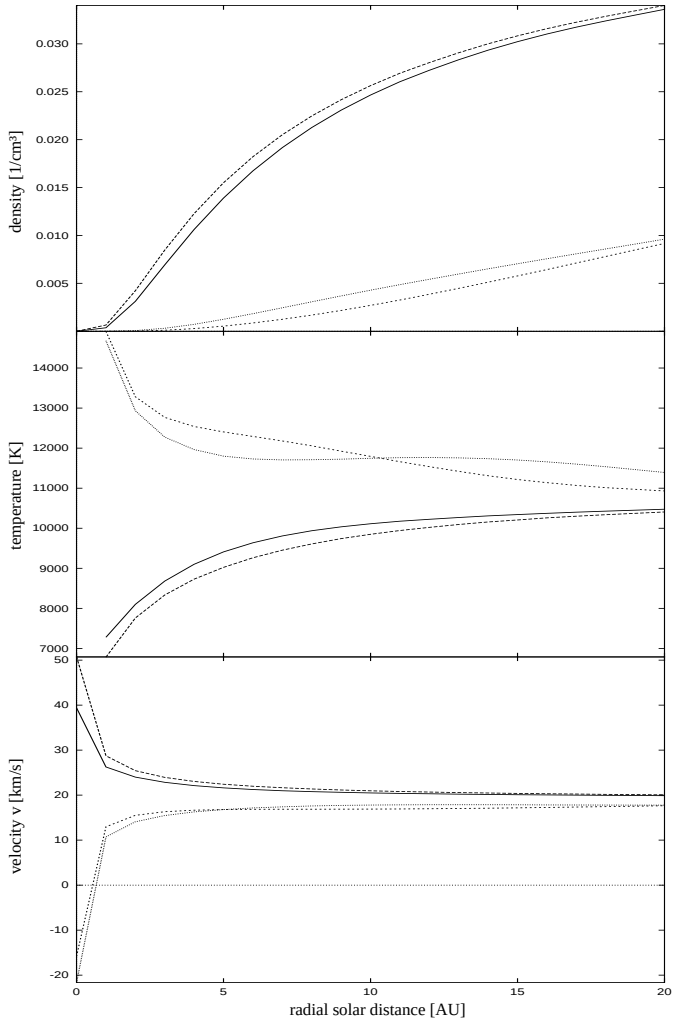

Fig. 2. Density, temperature and velocity (z-component) pattern of the Ruciński & Bzowski (1996, 1995) model (parameter set I Table 3) for two different times during the solar cycle 22. —— upwind direction 1994, – – – upwind direction 1996, - - - downwind direction 1994, ··· downwind direction 1996.

$$w_{\rm kin} = \left(\frac{m}{2\pi k}\right)^{3/2} \left[\frac{n_{0,dir}}{\sqrt{T_{x,dir}\,T_{y,dir}\,T_{z,dir}}} \exp\left[-\frac{m}{2k}\left(\frac{(v_x - v_{B,dir})^2}{T_{x,dir}} + \frac{v_y^2}{T_{y,dir}} + \frac{v_z^2}{T_{z,dir}}\right)\right] + \frac{n_{0,ind}}{\sqrt{T_{x,ind}\,T_{y,ind}\,T_{z,ind}}} \exp\left[-\frac{m}{2k}\left(\frac{(v_x - v_{B,ind})^2}{T_{x,ind}} + \frac{v_y^2}{T_{y,ind}} + \frac{v_z^2}{T_{z,ind}}\right)\right]\right] \quad (1)$$

with the use of the velocity vector saved previously. The parameters T, v_B and n_0 denote the temperature components, bulk velocity, and density of the respective populations in the reference region, respectively, and depend on the offset angle from the inflow direction. Alternatively, in the "no-interface" approach, a plain Maxwellian is used as distribution function of the gas in the reference region. The interface computations

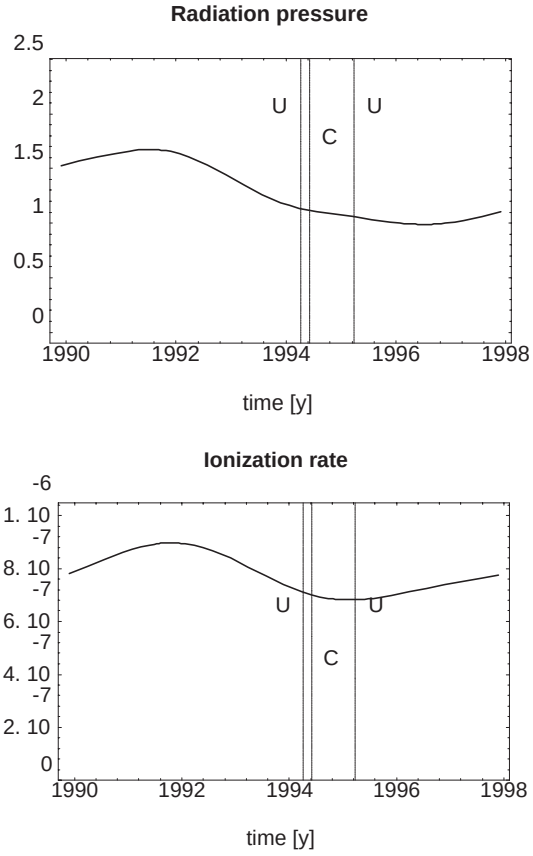

Fig. 3. The temporal course of radiation pressure in the units of solar gravity (*upper panel*) and the total ionisation rate (in s^{-1}) at 1 AU from the Sun during the time interval relevant for the HST observations. The vertical lines mark the actual times of HST observations used to comparison with the models; the lines marked with U correspond to the upwind lines of sight, the line marked with C corresponds to the crosswind line of sight.

were performed by V. Izmodenov for two sets of input parameters specified in Table 3.

To obtain the density, bulk velocity and temperature of the gas in the inner heliosphere, required by the radiation transport model, the local distribution function multiplied by the appropriate velocity moments is then integrated over velocity space (e.g. Bzowski et al. 1997 or Scherer et al. 1997) (see Fig. 2). Details and results of the modeling will be published elsewhere.

3.2. Radiation transport model

The radiation transport model by Scherer & Fahr (1996) is based on a hierarchical expansion of the well known time independent radiation transport equation (e.g.: Mihalas 1978). On the basis of the analytical and numerical concept of this model for solving the first and second order it is made evident that for heliocentric distances smaller than 5 AU the measurable IPM $H_{Ly\alpha}$ glow is clearly dominated by the first scattering order. All higher scattering orders are negligible when the actual local temperature and velocity patterns of the gas given by the hydrogen models and

Table 3. Two input parameter sets of the twin shock hydrogen model by Baranov & Malama (1993).

		Model I	Model II
LISM:			
proton density	cm^{-3}	0.095	0.07
velocity	$km\,s^{-1}$	25.3	25
temperature	K	7000	5672
H atom density	cm^{-3}	0.095	0.14
Mach number		2	1.6
Solar wind at Earth's orbit:			
proton density	cm^{-3}	8.7	7
velocity	$km\,s^{-1}$	450	450
temperature	K	130000	73507
Mach number		10	10
μ		1.28	0.75
net ionisation rate	s^{-1}	$7.8\ 10^{-7}$	$5.3\ 10^{-7}$

the angle/frequency–dependent partial photon redistribution in the scattering process is taken into account.

Only the long period time dependent effects in the hydrogen model, which do not influence the radiation transport code directly, were taken into account. In the radiation transport model the density, velocity and temperature given by the hydrogen model were treated as a static snapshot illuminated by the solar $H_{Ly\alpha}$ radiation source. As long as the fluctuations in the solar environment (e.g: solar activity, 27 day rotation period) are longer than about 24 hours, the treatment of the hydrogen pattern as fixed for the moment is a good approximation. But one has to take into account the actual hydrogen model and the actual solar line profile (see Sect. 4) to run the radiation transport model. For shorter time variations ($\tau \leq 27$ days) a new time–dependent radiation transport model would be needed which could take into account such conditions (e.g.: intensity fluctuations of the solar $H_{Ly\alpha}$ source by solar flares). This is because in this case the light travel time (100 AU $\sim$ 14 hours) for the passage of such a perturbation is of the same order as the duration of the perturbation itself. Taking into account non-isotropic, time varying emission of the solar source would enormously complicate the computations of the radiation transport model and make them hardly feasible.

In the literature there exist several alternative radiation transport models (e.g.: Keller et al. 1981, Quémerais & Bertaux 1993, Hall et al. 1993) but till now none of the models does take into account the variability in time of the solar $H_{Ly\alpha}$ emission profile. Also our model is not able to take care of time–variabilities of the solar $H_{Ly\alpha}$ emission profile but in contrast to most of the other radiation transport models it calculates spectral $H_{Ly\alpha}$ resonance emission profiles. Taking into account the local velocity and temperature pattern of the hydrogen, as given by the chosen density model, leads to a partial frequency redistribution of the solar line photons, absorbed and re–emitted by the neutral hydrogen. Caused by the partial redistribution in frequency space the resonantly absorbed first order photons are Doppler–shifted out of the line center by the individual velocity of the re–emitting atom, entroubling the next absorption process, i.e. second and higher scattering orders are gradually suppressed compared to situations where only complete frequency redistribution at line center is condsidered for the photon absorption and re–emission process. With the assumption of complete frequency redistribution, the higher scattering orders become much more important because a solar emission line photon, which will be absorbed resonantly in the line center, does not change its frequency by the re–emission process and still stays at line center where it is easily absorbed again. Therefore, for radiation transport models using the assumption of complete frequency redistribution of the absorbed and re–emitted photons the higher scattering orders naturally are more important relative to the first order than for models using partial frequency redistribution in describing the photon scattering conditions.

When comparing the results of radiation transport models taking into account partial frequency redistribution there still differences in the results of the multiscattering effects can be identified. But nevertheless, comparing e.g. the results of the Quémerais & Bertaux (1993) and our model, both taking into account partial frequency redistribution, in the vicinity of the sun at 1 AU where the HST spectra were taken, multiscattering effects in both models only play a minor role (Toma et al. 1997, Scherer & Fahr 1996) and the results of the two models, assuming a time independent solar line emission profile, are very similar.

When multiscattering effects can be excluded the discrepancies of the hydrogen glow results calculated with different radiation transport models are mainly caused by the different hydrogen pattern calculated by using different hydrogen models and due to the way these patterns are taken into account by the radiation transport models (e.g.: only taking into account the higher moments of distribution function or the distribution function itself).

A more detailed comparison of the spectra calculated with the two radiation transport models for interpreting the HST spectra can be found by Clarke et al., 1998).

3.3. Comparison of theoretical modelings with the HST data

Two sets of LISM and solar wind plasma parameters were used to compute the hydrogen models as inputs to the radiation transfer model (see Table 3). For both hydrogen sets the IPM hydrogen density, velocity and temperature patterns were calculated using the time–dependent hydrogen model for the dates when the HST spectra were observed. For the parameter set of model I (Table 3) a static case was also calculated for time independent, mean values for the radiation force and the hydrogen ionisation rate in the hydrogen model. Finally, an interface–free, but time–dependent hydrogen model was calculated for comparison purpose.

For every date when the HST data were observed, the hydrogen density, velocity and temperature snapshot relevant for that time moment, calculated using the hydrogen model and the

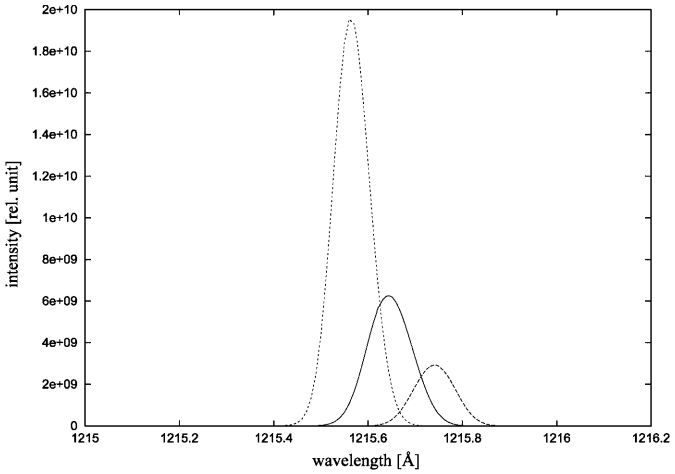

Fig. 4. $H_{Ly\alpha}$ glow spectra calculated with the radiation transport model by Scherer & Fahr (1996) using the results of the Ruciński & Bzowski (1995a, 1995b) hydrogen model (model I Table 3) at any given time, the position and line of sight of the HST when data were obtained. - - - data set 07.04.94 "upwind", —— data set 04.06.94 "crosswind", – – – data set 06.03.95 "downwind".

actual position and view direction of HST, were used by the radiation transport model for calculating $H_{Ly\alpha}$ glow spectra.

Since the HST data are very noisy (Fig. 1), it is not advised to deconvolve the GHRS PSF instrument function from the data. Therefore one cannot compare directly the spectral width of the HST data and the model, because the first is dominated by the PSF function (about a factor 2 broader (~ 0.1 Å) than the expected width of the $H_{Ly\alpha}$ glow spectra ($\sim$ Voigt profile with 8000 K)). Because the absolute full disk solar $H_{Ly\alpha}$ emission intensity for the dates of observations are not known either, also the spectral brightness could not be used to compare the theoretical models with the HST data. Therefore, in the following, we are only able to compare the shifts of spectral glow maximum off the $H_{Ly\alpha}$ line center λ_0 with the Doppler shift of the HST data after eliminating the component of the earth's orbital velocity along the line of sight (Table 2):

$$v_{\mathrm{IPM}} \;=\; \frac{\Delta\lambda}{\lambda_0} c$$

where

$$\lambda_0 \;=\; 1215.671\,\left[\text{Å}\right], c = 2.99793458\,10^5\,\left[\mathrm{kms}^{-1}\right].$$

These Doppler velocities are independent of the spectral brightness and are only weakly influenced by the GHRS PSF instrument function.

The velocities computed in that way are not the velocities of the LISM hydrogen far away from the sun but a sort of weighted average of velocity component of LISM hydrogen along the HST lines of sight after passing through the heliospheric interface.

4. Results

The Doppler velocities of the spectral maxima, calculated using the models described in the chapter before, and the Doppler velocities derived from the HST data are shown in Table 4. Because of the bad statistics of the HST downwind spectra only the two upwind spectra (07.04.94, 25.03.95) and the crosswind spectrum (04.06.94) could be used to compare the data with the models. The upwind data, collected at the same position and view direction of the HST but with a time interval of one year, show a shift in velocity of $3\,\mathrm{km\,s}^{-1}$. The HST crosswind spectrum shows a Doppler shift by $2.5\,\mathrm{km\,s}^{-1}$, reflecting the velocity component perpendicular to the neutral hydrogen inflow direction at infinity.

From Table 4 one can see that in the upwind direction low Doppler shifts of spectral lines observed upwind prevail. The observed velocities roughly correspond to the theoretical results from the models taking into account the decelerating effect of the heliospheric interface on the interstellar hydrogen gas. In contrast, the no-interface model with the same input parameters reflects a Doppler shift of ~ 3 km/s higher for the same lines of sight. From all the parameters of the hydrogen models used only the radiation pressure can decrease the bulk velocity of the gas close to the Sun. But decelerating the gas in the no-interface case to the velocity observed by HST would require a very high value of radiation pressure, which is not confirmed by observations of solar $H_{Ly\alpha}$ irradiance. Thus as first conclusion from this research one could say that from the employment of the most sophisticated hydrogen and radiation transfer models available it emerges the existence of a heliospheric interface decelerating the interstellar hydrogen.

As shown in Table 4, none of the models fits the data correctly. All of them show a Doppler velocity higher than the velocity measured by HST for both upwind spectra and the crosswind spectrum. Even when taking into account time–dependent hydrogen models it was impossible to reproduce the high velocity shift seen in the two HST upwind spectra. While in principle such a change in the inflow velocity owing to solar cycle effects cannot be excluded, the variation of hydrogen density, bulk velocity and temperature modeled for solar minimum, the period where the HST observations were performed, shows mild changes only (see Fig. 2). Thus, the time varying radiation pressure and ionisation rate during and a few years before the observations do not explain the change of the Doppler shift for the HST upwind spectra taken in a time span of one year.

The difference between the Baranov model I static, where mean stationary values for μ and β are used, and the Baranov model I time dependent is very small due to the fact that the radiation pressure and ionisation rate were positively correlated during observations, that is they were both going towards minimum. Since the decrease of radiation pressure accelerates the gas and the decrease of the ionisation rate leads to an increase of its velocity, their influences canceled each other. Thus, the distribution of density and velocity in this particular geometry and interval of time in the time-dependent case are quite similar to the static case.

The discrepancies between the model and observations most probably do not come from the neglect of the latitudinal dependence of the charge exchange rate in our models. The lines of sight observed by HST are located in the equatorial plane and

Table 4. Upper part of the Table: mean weighted hydrogen inflow speed calculated from the spectral maximum using different hydrogen models as input to the radiation transport model. The two lower parts of the Table: mean weighted hydrogen inflow speed calculated by using a static and a time–dependent hydrogen model, respectively, as input to the radiation transport model, but with two different, artificial $H_{Ly\alpha}$ profiles of the sun as emission source.

	upwind		crosswind	downwind	
	07.04.94	25.03.95	04.06.94	06.03.95	09.03.96
HST Data fit	$20.7\,km\,s^{-1}$	$24.3\,km\,s^{-1}$	$2.5\,km\,s^{-1}$	–[2]	–[2]
Baranov model I (static)	$23.2\,km\,s^{-1}$	$23.2\,km\,s^{-1}$	$3.5\,km\,s^{-1}$	$-20.2\,km\,s^{-1}$	$-20.2\,km\,s^{-1}$
Baranov model I	$23.2\,km\,s^{-1}$	$23.7\,km\,s^{-1}$	$3.9\,km\,s^{-1}$	$-20.2\,km\,s^{-1}$	$-20.2\,km\,s^{-1}$
Baranov model II	$24.2\,km\,s^{-1}$	$24.7\,km\,s^{-1}$	$3.5\,km\,s^{-1}$	$-23.7\,km\,s^{-1}$	$-23.2\,km\,s^{-1}$
No Interface	$27.1\,km\,s^{-1}$	$27.6\,km\,s^{-1}$	$1.9\,km\,s^{-1}$	$-27.1\,km\,s^{-1}$	$-27.1\,km\,s^{-1}$
Results with solar profile 2 (see text)					
Baranov model I (static)	$24.7\,km\,s^{-1}$	$24.7\,km\,s^{-1}$	$3.9\,km\,s^{-1}$	$-22.7\,km\,s^{-1}$	$-22.7\,km\,s^{-1}$
Baranov model I	$24.7\,km\,s^{-1}$	$25.2\,km\,s^{-1}$	$4.4\,km\,s^{-1}$	$-22.2\,km\,s^{-1}$	$-22.2\,km\,s^{-1}$
Results with solar profile 3 (see text)					
Baranov model I (static)	$22.2\,km\,s^{-1}$	$22.2\,km\,s^{-1}$	$3.5\,km\,s^{-1}$	$-18.7\,km\,s^{-1}$	$-18.7\,km\,s^{-1}$
Baranov model I	$22.2\,km\,s^{-1}$	$23.2\,km\,s^{-1}$	$3.9\,km\,s^{-1}$	$-18.7\,km\,s^{-1}$	$-18.7\,km\,s^{-1}$

[1] Values corrected by earth velocity component along the HST line of sight (see Table 2).
[2] Bad statistics. No reliable fit possible.

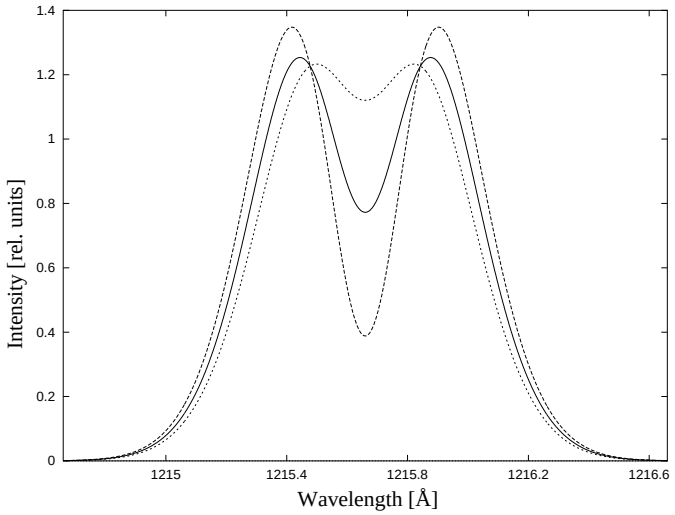

Fig. 5. $H_{Ly\alpha}$ emission line of the sun. —— standard solar profile (fit to OSO 8 data), normally used in the radiation transport model of this paper; – – – model profile 2 (see text); - - - model profile 3 (see text). The area under the curves of the profiles are scaled to 1.

upwind hemisphere, where this effect should not significantly influence the gas distribution.

The source of such a short time scale changing effect could possibly be the solar $H_{Ly\alpha}$ emission line profile. The $H_{Ly\alpha}$ line of the sun is a self–inverted emission line and could vary at a time scale of a few days or shorter (Vidal–Madjar 1975). In the radiation transport model by Scherer & Fahr (1996) a time independent fit of the solar emission profile measured by the OSO 8 satellite (Bonnet et al. 1978) is used as source for the solar $H_{Ly\alpha}$ line. Till now a detailed analysis of the time varying self–inverted part of the solar $H_{Ly\alpha}$ emission line has not been presented (see also Toma et al. 1997). Therefore, to check the influence of the $H_{Ly\alpha}$ emission line profile on the Doppler velocities calculated with the radiation transport model, two model line profiles were used (see Fig. 5) and the Doppler velocities related to the HST data were derived (Table 4 model profile 2, 3).

The Doppler velocities calculated with the solar $H_{Ly\alpha}$ profiles I and II differ by $2.5\,km\,s^{-1}$ in the upwind and downwind direction while the computed Doppler velocities into the crosswind direction differ only slightly. Different parts of the hydrogen distribution function in the velocity space, acting as sources of re-emission, are illuminated by different parts of the artificial, self-inverted solar H Ly-α line used here for the test. Therefore, into the upwind and downwind directions different solar $H_{Ly\alpha}$ emission lines cause different shifts in $H_{Ly\alpha}$ glow profiles. The crosswind glow spectra are only weakly influenced by the solar emission profile in the Doppler shift but strongly in the absolute intensity because in the crosswind direction the projection of the local bulk velocity of the gas on the line of sight is always small, and thus only the central part of the solar H Ly-α line is responsible for the glow intensity.

It is remarkable that the deeper the self–inversion of the solar $H_{Ly\alpha}$ emission line, the more sensitive is the $H_{Ly\alpha}$ glow to small differences of the neutral hydrogen velocity pattern (see Table 4 Baranov model I for the model solar profiles I and II). In the vicinity of the line center (± 0.2 Å), which is the main part of the solar source profile responsible for the hydrogen resonance glow (hydrogen inflow speed of $20\,km\,s^{-1}$ is equivalent to a spectral shift by about 0.1 Å), in case of a deep self–inverted profile small Doppler shift lead to stronger changes in the source brightness than in the case of a shallow self–inverted source emission line.

5. Conclusion

We have carried out an analysis of the GHRS HST $H_{Ly\alpha}$ glow spectra observed in the time period of 1993 to 1996. We used a hydrogen model taking into account time–dependent effects due to solar cycle and alternatively including or excluding the modification of the LISM gas by the heliospheric interface.

The first conclusion is that while no completely satisfactory agreement between the model and the data could be achieved, generally better results are given by the model that includes the influence of the interface and thus the existence of the interface can be confirmed from the HST observations of the hydrogen backscattered radiation.

In the period of solar minimum, when the data were collected, the time–dependent hydrogen model only shows weak variations during one year, and hence the different spectral shifts of the hydrogen $H_{Ly\alpha}$ glow measured with the GHRS HST instrument in the upwind direction between 1993 and 1996 could not be explained. All theoretical models, used here for a time–dependent analysis, differs at least about $0.5\,\mathrm{km\,s^{-1}}$ by comparison with the data. The solar $H_{Ly\alpha}$ emission profile, which possibly changes on time scales of days or months, strongly affects the Doppler shift of the interplanetary $H_{Ly\alpha}$ emission spectra and hence must be taken into account in the future analysis. More research on the time dependent behavior of the solar $H_{Ly\alpha}$ line profile and especially its self–inverted line center is needed.

Another possible reason of the remaining discrepancies could be still a LISM magnetic field inclined to the hydrogen inflow direction and causing a tilting of the interface symmetry axis. A squeezed interface structure would then be established as result of magnetohydrodynamic stress forces and this would fake a tilt of the "real" hydrogen inflow direction (see details in Scherer et al. 1997).

Summarizing, it is shown by the endeavors of this paper that the GHRS HST $H_{Ly\alpha}$ glow spectra are very appropriate for studying the interplanetary hydrogen pattern. New GHRS HST $H_{Ly\alpha}$ glow measurements with improved signal–to–noise ratios would be helpful. Not only fixed at three view directions (upwind, crosswind, downwind) but a circular scan from the upwind to the downwind direction (resolved with about 8 to 10 spectra) with an improved count statistics taken in a period of several days and measured again after a time delay of 2–3 years would be ideal. Especially now, in the beginning of the active solar phase, when the hydrogen models show stronger time effects on the hydrogen distribution than during the minimum period, this would help to fix the LISM hydrogen parameters. Additionally, this would be supported by improved data statistics, when a relevant analysis also of the downwind spectra becomes possible. Also in the near future, as mentioned above, research on the fluctuation of the solar $H_{Ly\alpha}$ line center is needed which possibly could be done by data of the SUMER experiment on–board the SOHO satellite (Wilhelm et al. 1995, Lemaire et al. 1998).

Acknowledgements. The authors thank Dr. Vlad Izmodenov who performed the Baranov & Malama model calculations for the needs of this research. They also thank Dr. John Clarke who provided them with the HST GHRS $H_{Ly\alpha}$ glow data. The full-disk line-integrated, re-calibrated time series of the solar Lyman-α flux were made available to us by Dr. W. Kent Tobiska, the IMP 8 data were provided by the MIT Space Plasma Physics Group and are publicly available by ftp or the WWW and the 10.7 cm data were downloaded from the publicly available FTP Archive of the US Dept. of Commerce/NOAA/NESDIS National Geophysical Data Center. This research was performed in the collaboration between the Institut für Extraterrestrische Forschung der Universität Bonn and the Space Research Centre of the Polish Academy of Sciences as part of the joint project "Physics in the outer heliosphere – theory and observations" (DFG 436/POL/113/80), carried out in the framework of cooperation between the Deutsche Forschungsgemeinschaft and the Polish Academy of Sciences. The work of D.R. and M.B. was supported by the research grant No.2 P03C 013 11 from the Committee for Scientific Research (Poland).

References

Ajello J.M., Stewart A.I., Thomas G.E., Graps A., 1987 ApJ 317, 964
Ajello J.M., Pryor W.R., Barth C.A. et al., 1994, A&A 289, 283
Baranov V.B., Malama Y.G., 1993, J.Geophys. Res. 98, 157
Baum S., 1994, HST Data Handbook, Version 1.0 (Space Telescope Science Institute Baltimore, Maryland
Bertaux J.L., Lallement R., Kurt V.G., Mironova E.N. 1985, A&A 150, 1
Bertaux J.L., Quémerais E., Lallement R., 1996, Geophys. Res. Letters, Vol. 23 No 25 3675
Bertin P., Lallement R., Ferlet R., Vidal–Madjar A., 1993, JGR Vol 98 No A9, 193
Bonnet R.M., Lemaire P., Vial J.C., et al., 1978, ApJ 221, 1032
Bzowski M., Ruciński D., 1995a, Sp. Science Rev. 72, 467
Bzowski M., Ruciński D., 1995b, Adv. Space Res. 16 No. 9, 131
Bzowski M., Fahr H.J., Ruciński D., Scherer H., 1997, A&A 326, 396
Clarke J.T., Lallement R., Bertaux J.-L., Quémerais E., 1995, ApJ 448, 893
Clarke J.T., Lallement R., Bertaux J.-L., et al., 1998, ApJ 499, 482
Fahr H.J. 1996, Space Science Rev. 78, 199
Fahr H.J., Ripken H.W., 1984, A&A 241, 251
Gilliland R.L., Morris S.L., Weymann R.J., Ebbets D.C., Lindler D.J., 1992, PASP 104, 367
Hall D.T., Shemansky D.E., Judge D.L., Gangopadhyay P., Gruntman M.A. 1993, J.Geophys.Res. 98, 185
Kausch Th., Fahr H.J., 1997, A&A 325, 828
Keller H.U., Thomas G.E., 1979, A&A 80, 227
Keller H.U., Richter K., Thomas G.E., 1981, A&A 102, 415
Kyrölä E., Summanen T., Råback P., 1994, A&A 288, 299
Mihalas D., 1978, Stellar atmospheres, second edition, W.H. Freeman and Company San Francisco
Lallement R., 1989, Cospar Colloquia Series Vol 2, Solar Wind 6, Ed. E.Marsch and R.Schwenn
Lallement R., 1990, Cospar Colloquia Series Vol. 1, Physics of the outer heliosphere, Ed. S. Grzędzielski, D.E. Page
Lallement R., 1993, Adv. Space Res. Vol. 13, No 6, 113
Lallement R., Bertaux J.L. 1985, A&A 150, 21
Lallement R., Bertaux J.L., Sandel B., Chassefière E., 1990a, Cospar Colloquia Series Vol. 1, Physics of the outer heliosphere, Ed. S. Grzędzielski, D.E. Page
Lallement R., Bertaux J.L., Chassefière E., Sandel B., 1990b, Cospar Colloquia Series Vol. 1, Physics of the outer heliosphere, Ed. S. Grzędzielski, D.E. Page

Lallement R., Bertaux J.L., Chassefière E., Sandel B., 1991, A&A 252, 385
Lemaire P., Emerich C., Curdt W., Schühle U., Wilhelm K., 1998, A&A 334, 1095
Osterbart R., Fahr H.J., 1992, A&A 264, 260
Press, W.H., Rybicki, G.B., 1989, ApJ 338, 277-280
Quémerais E., Bertaux J.L. 1993, A&A 277, 283
Quémerais E., Lallement R., Bertaux J.L. 1992, A&A 265, 806
Quémerais E., Bertaux J.L., Sandel B.R., Lallement R., 1994, A&A 290, 941
Quémerais E., Sandel B.R., Lallement R., Bertaux J.L., 1995, A&A 299, 249
Ripken H.W., Fahr H.J., 1983, A&A 122, 181
Ruciński D., Bzowski M., 1995, A&A 296, 248
Ruciński D., Bzowski M., 1996, Sp. Science Rev. 78, 265
Ruciński, D., Cummings, A.C., Gloeckler et al., 1996, Space Sci. Rev. Vol. 78, pp 73–84
Scherer H., Fahr H.J., 1996, A&A 309, 957
Scherer H., Fahr H.J., Clarke J.T., 1997, A&A 325, 745
Solderblom D.R., 1994, Instrument Handbook for the Goddard High Resolution Spectrograph (GHRS), Version 5.0, Space Telescope Science Institute Baltimore, Maryland
Summanen T., 1996, A&A 314, 663
Summanen T., Lallement R., Bertaux J.L, Kyrölä E., 1993, JGR Vol 98 No A8, 213
Tobiska W.K., Pryor W.R., Ajello M., 1997, JGR Vol. 24, No. 9, 1123
Toma G., Quémerais E., Sandel B.R., 1997, A&A 491, 908
Williams L.L., Pauls H.L., Zank G.P., 1996, "Solar Wind 8", 609
Vidal–Madjar A., 1975, Solar Physics 40, 69–86
Wilhelm K., Curdt W., Marsch E. et al., 1995, Solar Physics 162,189
Zank G.P., Pauls H.L., 1996, Sp. Science Rev. 78,95